Dislocation stress-velocity dependence in alloys

R. B. Schwarz
Materials Science Division, Argonne National Laboratory, Argonne, Illinois 60439
(Received 8 January 1980)

The frictional stress $\sigma(v)$ is calculated for a dislocation gliding at an average velocity v on a plane containing a fixed random distribution of weak obstacles of finite interaction range, in the presence of viscous forces. For *very low-viscous forces* the dislocation travels quasistraight, overcoming each obstacle independently of the relative positions of the other ones. Dislocation glide is possible only for $v \gtrsim \frac{1}{50} v_s$, where v_s is the sound velocity in the solid. The frictional stress has the usual viscous drag component plus an extrinsic component proportional to the solute concentration, which vanishes asymptotically for $v >> \frac{1}{50} v_s$. For *high-viscous forces*, glide is possible at all velocities for stresses above a critical stress σ_c. For $\sigma \approx \sigma_c$ the motion is sensitive to the obstacle statistics. For $\sigma \gtrsim 2\sigma_c$ the motion is mostly drag controlled, with characteristics similar to those observed in the presence of low-viscous forces.

I. INTRODUCTION

A dislocation gliding at an average velocity v through a crystalline solid free of localized obstacles and Peierls potential encounters a viscous drag characterized by an intrinsic damping constant B. To maintain the motion requires an applied shear stress

$$\sigma = Bv/b \quad . \tag{1}$$

In general, B is thought to include contributions from the scattering of phonons and electrons. For a nonuniform speed, there is additional drag due to the radiation of acoustic waves.

In solids containing weak localized obstacles, the dislocation motion changes in character depending on the value of σ and the temperature T. At $T=0$ K, no motion occurs if σ is smaller than a critical stress σ_c, while for $\sigma > \sigma_c$, the dislocation moves continuously, experiencing, in general, a frictional stress larger than the (intrinsic) viscous force given by Eq. (1). For $T>0$ and $\sigma \lesssim \sigma_c$ the motion is jerky, with the dislocation spending a fraction of the time awaiting thermally activated release from strong configurations of obstacles, and the rest of the time moving between these obstacle configurations. For $T>0$ and $\sigma \gtrsim \sigma_c$, the dislocation motion is again continuous, with characteristics similar to those for $T=0$.

Two (extrinsic) dissipative mechanisms have been recognized for moving dislocations in alloys: (a) the excitation of localized lattice vibrations associated with the solute atoms,[1] and (b) the generation of dislocation vibrations (due to interaction of the dislocations with the fixed solute atoms) which then dissipate their energy into the lattice through the intrinsic damping mechanisms.[2] Within certain velocity regimes these extrinsic mechanisms have a predicted contribution to the flow stress in alloys which is proportional to the first power of the solute concentration, c (whereas, for dilute alloys, $\sigma_c \propto \sqrt{c}$). It has been recently suggested by Nabarro, Basinski, and Pascual[3] that this contribution alone is responsible for the linear concentration dependence of the flow stress found in constant-strain-rate experiments on Cu-Al and Cu-Si alloys at $T=470$ K.[4]

Only the second extrinsic dissipation mechanism mentioned above is considered here; as discussed in Sec. V D, it should be much more important than the former, especially for the dislocation velocities to be expected in the plastic deformation of alloys. Frost and Ashby[5] also considered this type of energy loss, but for the particular physical model of a square array of pointlike obstacles (zero interaction range) in the presence of high viscous forces (no dynamic effects). Kocks, Argon, and Ashby[6] calculated the flow stress for a dislocation running into a linear barrier in the presence of low and high viscous forces. The present work considers the motion of a dislocation through the more realistic model of a random two-dimensional array of obstacles of finite interaction range, in the presence of both low- and high-viscous forces. The problem of a moving dislocation colliding with an isolated obstacle of finite interaction range is considered first. The flow stress $\sigma(v)$ for a random distribution of obstacles is then obtained by a generalization of the previous result under the assumption of independent collision events. This assumption is expected to always be valid for $\sigma >> \sigma_c$. The flow stress is also calculated exactly by a dynamic computer simulation, using a computer code developed previously.[7,8] A comparison of these two results determines the extent to which the collision events can be considered independent.

The calculations are performed using a set of nor-

malized coordinates (Sec. II) that were introduced earlier.[7,8] These coordinates provide two advantages: the analytic form of the results is greatly simplified, and numerical calculations need to be executed only for a small number of parameter values.

II. NORMALIZED COORDINATES

Consider a dislocation gliding on a plane containing a random distribution of weak obstacles (interaction forces much smaller than the dislocation line tension). The dynamic equation of motion in an xy coordinate system with the x axis oriented along the dislocation requires the specification of several parameters: m, mass per unit dislocation length; B, intrinsic viscous damping; Γ, dislocation line tension; f_0, strength of the dislocation-obstacle interaction force in units of twice the line tension (here $f_0 \ll 1$); y_0, range of the interaction in the direction perpendicular to the average dislocation direction; $l_s \approx b/\sqrt{c}$, average separation between the obstacles on the glide plane; and c, solute molar fraction.

The number of independent parameters is reduced and the calculations are substantially simplified by working in the following normalized coordinates (Refs. 7 and 8):

$$\xi = (x/l_s)\sqrt{f_0} \ , \tag{2a}$$

$$\eta = (y/l_s)/\sqrt{f_0} \ , \tag{2b}$$

$$\theta = (t/l_s)(\Gamma f_0/m)^{1/2} \ . \tag{2c}$$

In these coordinates, the dislocation behavior in the constant line-tension approximation is described by

$$\frac{1}{2}\frac{\partial^2\eta}{\partial\theta^2} + \gamma\frac{\partial\eta}{\partial\theta} - \frac{1}{2}\frac{\partial^2\eta}{\partial\xi^2} = S + \sum g\left(\frac{\eta-\eta_i}{\eta_0}\right)\delta(\xi-\xi_i) \ , \tag{3}$$

where the sum extends over all obstacles interacting with the dislocation. The normalized damping γ and the normalized applied stress S are, respectively,

$$\gamma = Bl_s/(4\Gamma m f_0)^{1/2} \tag{4}$$

and

$$S = \sigma b l_s/(2\Gamma f_0^{3/2}) \ , \tag{5}$$

the normalized interaction range, η_0, follows from Eq. (2b) with $y = y_0$; the term $g[(\eta-\eta_i)/\eta_0]$ describes the interaction between the dislocation and an obstacle located at (ξ_i, η_i); and δ is the Dirac δ function. In these coordinates, the mass density and the line tension are both $\frac{1}{2}$. The normalized obstacle density and the normalized obstacle strength are both unity. The normalized velocity of a wave front traveling in the $\pm\xi$ direction along the dislocation is unity. The normalized velocity V of the dislocation (in the η direction) is

$$V = (v/v_s)(1/f_0) \ , \tag{6}$$

where $v_s = (\Gamma/m)^{1/2}$ is the shear-wave velocity in the solid. In the absence of viscous damping ($\gamma = 0$), a point force applied to the dislocation produces a proportional change in the local dislocation velocity. The proportionality constant defines the dislocation wave impedance Z. The wave impedance of a dislocation line[9] extending to $\pm\infty$ is $Z = 2(\Gamma m)^{1/2}$. Therefore, the normalized velocity V gives the physical velocity v in units of the maximum velocity change, $v_s f_0 = 2\Gamma f_0/Z$, that an obstacle of strength $2\Gamma f_0$ can impose locally on the dislocation. In our normalized coordinates the wave impedance is unity.

III. CALCULATIONS

To start the long-range motion of a dislocation through a random field of obstacles in the absence of thermal fluctuations requires the application of a critical normalized stress S_c ($S_c \approx 1$; Refs. 7 and 8). For $S > S_c$ the motion is continuous. The dislocation receives a pair of impulses as it crosses over the interaction force field of each obstacle. These impulses generate a pair of disturbances on the dislocation, which leave the collision site propagating in opposite directions at the speed of sound (Fig. 1). The duration of the collisions, and hence the strength of the impulses, decreases as the applied stress and average velocity increase. Therefore, for $S \gg S_c$ the dislocation travels essentially straight at an average steady-state velocity near the drag-limited velocity S/γ (velocity $\sigma b/B$ in physical units). Relativistic effects expected for velocities approaching the speed of sound are assumed to be included in the value of B.

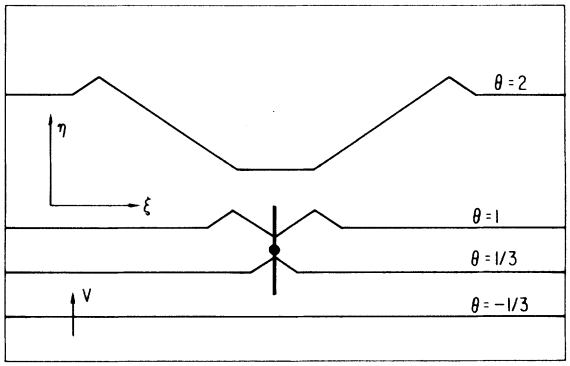

FIG. 1. Successive positions of an initially straight dislocation gliding at speed $V > 1$ in the absence of friction ($\gamma = 0$), which at $\theta = 0$ collides with an obstacle having the attractive interaction profile of Fig. 2(a).

The dislocation behavior in normalized units is described by Eq. (3). Let V_0 be the steady-state average dislocation velocity under the applied stress S ($S >> S_c \approx 1$). We consider next a unit length of dislocation and perform a time average of Eq. (3) between times θ_1 and θ_2, with $V_0(\theta_2-\theta_1) >> 1$. This last condition ensures that the forward dislocation displacement during $\theta_2-\theta_1$ is large compared to the average separation between obstacles. Since, as discussed above, for $S >> S_c$ the dislocation remains (on the average) parallel to the ξ axis and moves at a uniform velocity, this gives

$$S=\gamma V_0+\frac{1}{V_0(\theta_2-\theta_1)} \times \sum_i{}' \int_{\theta_1}^{\theta_2} -V_0 g\left[\frac{\eta(\theta)-\eta_i}{\eta_0}\right] d\theta \ . \tag{7}$$

where $\sum'$ denotes a sum over all obstacles contained within a ribbon of glide plane having width unity (in the ξ direction) and length $V_0(\theta_2-\theta_1)$ (in the η direction). Since the normalized obstacle density is one, this sum has $V_0(\theta_2-\theta_1)$ terms. Therefore, the integral in Eq. (7) can be identified with the average increment in flow stress per obstacle, which adds to the normal viscous-flow-stress component, γV_0. By considering the similar problem of an obstacle running at a velocity $-V_0$ into a stationary dislocation, it is seen that the integral in Eq. (7) equals the work done by the applied force necessary to keep the obstacle moving at the prescribed velocity $-V_0$. In the present case of the moving dislocation, this work is done by the applied stress. In both cases it is initially stored as kinetic and potential energy of the two elastic perturbations propagating on the dislocation, which then dissipates into the lattice through the viscous damping.

As a result of all previous collisions, the velocity of the dislocation at any point along its length is $V_0+V_1(\theta)$, where $V_1(\theta)$ is a random function of time with an average value of zero. If the flow-stress contribution of each obstacle depends on $V_1(\theta)$ and on the relative positions of the other obstacles, the evaluation of Eq. (7) is best achieved through a dynamic computer simulation,[8] which performs the necessary statistical averaging. This will be done in Sec. III B. In what follows we calculate the flow stress for isolated collision events, assuming that each obstacle contributes equally to the flow stress. From the previous discussion, it is manifest that this assumption should work best for high applied stresses (e.g., $S >> S_c$, where $V_0 >> V_1$). The extent to which the assumption of isolated collisions is applicable to lower applied stresses will become apparent from a comparison of these calculations with the exact results obtained through the dynamic computer simulation.

A. Flow stress for isolated collision events

We consider next that as the dislocation reaches each obstacle, it is straight and moving at the average velocity V (we henceforth drop the subindex zero from V_0). It then follows from Eq. (7) that

$$S=\gamma V+\Delta W \ , \tag{8a}$$

where

$$\Delta W(\eta_0,\gamma,V)=\int_0^{\Delta\theta} V g\left[\frac{\eta(\theta)-\eta_i}{\eta_0}\right] d\theta \tag{8b}$$

is the energy initially stored as traveling perturbations on the dislocation as a result of its collision with an isolated obstacle located at ($\xi=0$, $\eta=\eta_i$). The dislocation first contacts the obstacle interaction range at $\theta=0$ and leaves it at $\theta=\Delta\theta$. In what follows we integrate Eq. (8b) separately for the limiting case of $\gamma\to 0$ and for the case of a finite damping value. Only the first case gives simple analytic forms.

1. *Very low viscous damping* ($\gamma << 1$)

When $\gamma=0$, the application of a point force on the dislocation produces a proportional change in the local dislocation velocity. The proportionality constant is the dislocation wave impedance, which in our normalized units is unity (Sec. II). Therefore, as the dislocation surmounts an obstacle, $d\eta/d\theta=V+g(s)$, where $s=[\eta(\theta)-\eta_i]/\eta_0$. After a short mathematical manipulation, Eq. (8) gives

$$S=\gamma V+\eta_0 V\int_{-1}^{1}\frac{-g(s)}{V+g(s)}\,ds \ . \tag{9}$$

Even though in the above expression the extrinsic losses have been calculated for $\gamma=0$, we expect this expression of S to hold for $0<\gamma<<1$ (see also Sec. III A 2 below). Since $|g(s)|\leq 1$ (Sec. II), Eq. (9) gives a finite S value only for $V>1$. In the present model, when $V\leq 1$ the dislocation is not able to surmount any of the obstacles because $d\eta/d\theta$ becomes zero some time after the dislocation contacts the obstacle. It is easily shown that, provided the interaction force profile is antisymmetric [$g(s)=-g(-s)$], repulsive and attractive obstacles give the same flow stress in Eq. (9).

Equation (9) can easily be integrated for the simple interaction force profiles of Figs. 2(a) and 2(b): (i) Square interaction profile [Fig. 2(a)][10]

$$S=\gamma V+\eta_0 2V/(V^2-1) \ . \tag{10}$$

and (ii) triangular interaction profile [Fig. 2(b)]

$$S=\gamma V+\eta_0\{V^2\ln[(V+1)/(V-1)]-2V\} \ . \tag{11}$$

For more complicated interaction profiles, such as

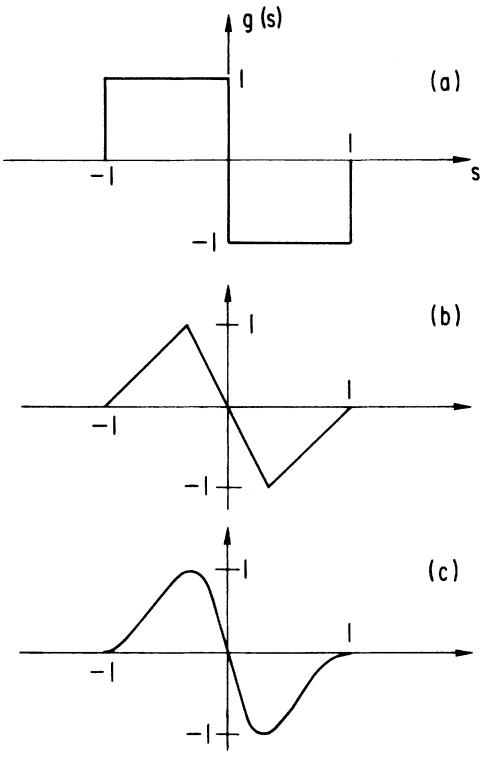

FIG. 2. Profiles for the dislocation-obstacle interaction force used in the calculations. $s=(\eta-\eta_i)/\eta_0$, where η_i is the ordinate of the center of the obstacle and η_0 in the interaction range. The profiles shown correspond to attractive interactions [see Eq. (3)]. For profile 2(c), $g(s)=As(1-s^2)^2$, with $A=\frac{25}{16}\sqrt{5}$.

the one shown in Fig. 2(c), $S(V)$ can be obtained by a numerical integration of Eq. (9).

2. *Finite viscous forces*

When γ is finite, the change in local dislocation velocity at the collision site ($\xi=0$) is no longer proportional to the dislocation-obstacle interaction force. In order to calculate ΔW in Eq. (8b) we need to solve first for $\eta(\xi=0,\theta)$.

The Green's function[11] for the attenuated string equation [Eq. (3)], giving the response of a dislocation to a force $\delta(\xi)\delta(\theta)$, is

$$G(\xi,\theta)=[u_0(\xi+\theta)-u_0(\xi-\theta)]\times\exp(-\gamma\theta)I_0[\gamma(\theta^2-\xi^2)^{1/2}] \quad , \quad (12)$$

where u_0 is the unit step function (zero for a negative argument and unity otherwise) and I_0 is the modified Bessel function of zero order. Superimposing the dislocation response to the interaction force $g(s(\theta))\delta(\xi)$ onto the motion prior to the collision, and integrating with respect to ξ, gives

$$\eta(\xi=0,\theta)=V\theta+\int_0^\theta g(s(\theta'))e^{-\gamma(\theta-\theta')}\times I_0[\gamma(\theta-\theta')]\,d\theta' \quad , \quad (13a)$$

where

$$s(\theta)=[\eta(\xi=0,\theta)-\eta_0]/\eta_0 \quad . \quad (13b)$$

Here $\theta=0$ corresponds to the instant the dislocation first touches an obstacle centered at $(0,\eta_0)$. This integral equation was solved numerically for selected values of η_0 and γ. With $\eta(\xi=0,\theta)$ known, ΔW was calculated from Eq. (8b) (also numerically) and S was evaluated as $S=\gamma V+\Delta W$. The results will be presented in Sec. IV.

B. Flow stress for a random planar distribution of obstacles

The $V(S)$ dependence for a dislocation gliding through a random distribution of obstacles was obtained by computer simulation, using a previously developed computer code.[7,8] In this method the dislocation position is obtained as a function of space and time by performing a numerical integration of the dynamic equation of motion [Eq. (3)] under a constant applied stress. The old code was slightly modified by removing the periodic boundary conditions of the obstacle field in the direction of motion. For this, a new obstacle field (Poisson distribution) was continuously generated in front of the moving dislocation. For a given S value, the velocity V was calculated from the time spent by the dislocation in crossing a large area of the glide plane containing >2000 obstacles. Other details of the computer simulation have been published previously.[8] The results are presented in Sec. IV.

IV. RESULTS

A. Results for $\gamma \ll 1$

Figure 3 shows the results of the calculations and of the computer simulations for $\gamma=0.1$ and the triangular interaction profile of Fig. 2(b) with $\eta_0=0.5$. The two calculations assuming independent collision events [solid curve given by Eq. (11) and open circles resulting from the numerical integration of Eqs. (13) and (8)] give the same results, showing that for $\gamma<0.1$ the extrinsic contribution to the flow stress, ΔW, is largely independent of γ. The calculated $S(V)$ curves are multivalued in V. This derives from the fact that while the intrinsic contribution to the flow stress, γV, decreases linearly with decreasing V, the extrinsic contribution, ΔW, increases much faster

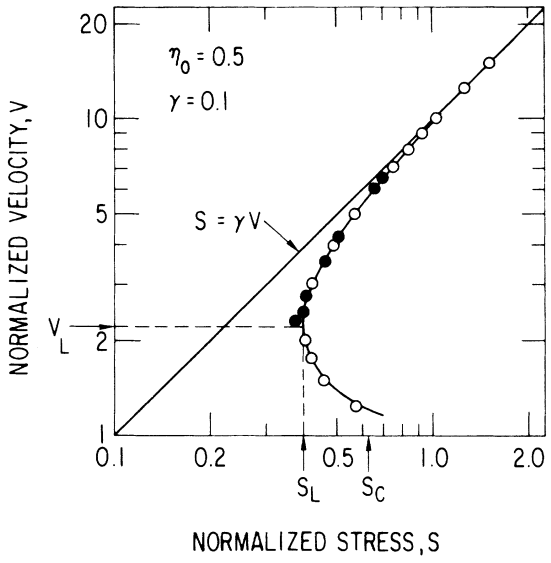

FIG. 3. Velocity-stress dependence (normalized units) for $\gamma = 0.1$ and the triangular interaction profile of Fig. 2(b) with $\eta_0 = 0.5$. The solid curve is Eq. (11). The open symbols are numerical calculations using Eqs. (13) and (8). The solid symbols are computer simulation results for random arrays of obstacles. The velocity regime $1 < V < V_L$ is unaccessible to dislocations under a constant applied stress.

as V decreases and approaches unity. It should be noted, however, that the calculations were performed by prescribing an average dislocation velocity, rather than under the more plausible condition of a prescribed applied stress (used in the computer simulations). The minimum value of S in the calculated $S(V)$ curve defines $S_L(\eta_0, \gamma)$ and $V_L(\eta_0, \gamma)$.

The computer simulations showed, in agreement with previous simulations,[8] that under a slowly increasing applied stress a stationary dislocation does not start moving until S reaches a critical value $S_c \simeq 0.63$, which is *larger* than S_L (Fig. 3). The dislocation then acquires the velocity $V(S_c)$ given by the *upper* branch of the calculated $V(S)$ curve. If, once the dislocation is in motion, the applied stress is slowly decreased, the motion stops when $S \approx S_L$. Therefore, under conditions of constant applied stress, the lower branch of the calculated $S(V)$ curve (i.e., $V < V_L$) is inaccessible to the dislocations in the simulations and, presumably, to real dislocations.

A detailed analysis of the computer simulations revealed that while the dislocation is in motion it remains essentially straight over the length $30l_s$ used in our simulations (periodic boundary conditions in the ξ direction; see Ref. 8) and overcomes each obstacle independently of the position of the others. This and the excellent agreement found between the calculations and simulations indicates that for $\gamma \ll 1$ the collisions can indeed be considered independent.

The regime $\gamma \lesssim 1$, where $S_c > S_L$, has been identified[8] with underdamped dislocations and "inertial effects."[12,13] The present results show that in this low-viscosity regime, dislocations either move at high velocities [$V \geq V_L(\eta_0, \gamma) > 1$] or do not move at all. Calculations performed with $\gamma \ll 1$, with other obstacle profiles and for other values of η_0 produced results qualitatively similar to those discussed above. The agreement between the calculations and the simulations was always very good except for the largest η_0 values ($\eta_0 > 2$), where the simulations showed that the motion could continue under applied stresses and velocities $\sim 10\%$ lower than the calculated S_L and V_L values.

B. Results for $\gamma \gtrsim 2$

The $V(S)$ dependence obtained for obstacles having the smooth interaction profile of Fig. 2(c) with two different values of η_0 and $\gamma = 3$ are shown in Fig. 4. The dashed curves give $V(S)$ calculated under the assumption of independent collision events [numerical integration of Eqs. (13) and (8)] and the solid symbols are the computer simulation results. The calculated $V(S)$ dependence is qualitatively similar to that obtained for $\gamma \ll 1$. By analogy with the results

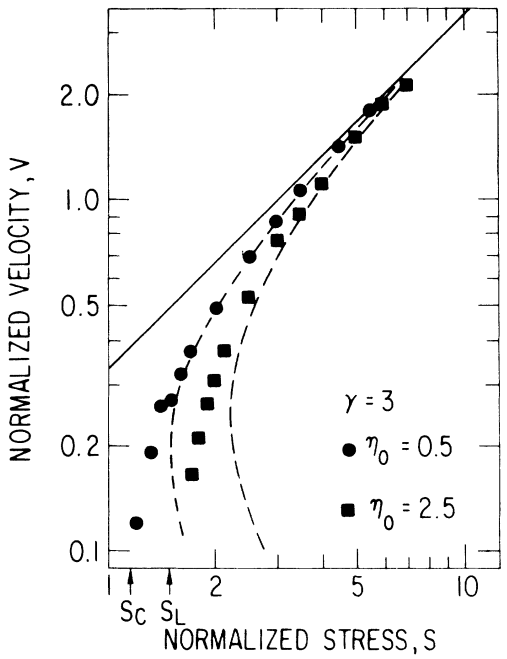

FIG. 4. Velocity-stress dependence (normalized units) for a dislocation interacting with obstacles having the smooth interaction profile of Fig. 2(c). Solid symbols: computer simulation results for random arrays of obstacles. Dashed curves: calculated values from Eqs. (13) and (8). The solid line gives the viscous drag component. Arrows show S_c and S_L for $\eta_0 = 0.5$ only.

for $\gamma << 1$ (Fig. 4), and for the sake of further discussion, we define $S_L(\eta_0, \gamma)$ as the lowest value of S given by the *calculated* $S(V)$ curve. The computer simulation results coincide with the calculations only at high velocities, where the flow stress is due mainly to intrinsic losses. For these velocities, the simulations show that the dislocation travels quasistraight, surmounting each obstacle independently of the position of the neighboring ones, in complete analogy with the motion for $\gamma << 1$. Under a decreasing applied stress, the extrinsic losses increase but, contrary to the case of $\gamma << 1$, the dislocation does not stop at the corresponding $S_L(\eta_0, \gamma)$ stress. The computer simulations show that under this applied stress the dislocation cannot find a configuration of obstacles strong enough to hold it in a *quasistraight* position. As S is further decreased, the motion becomes highly nonuniform, with sections of the dislocation moving ahead of the rest, percolating first through regions of lower obstacle densities. The average velocity V remains a continuous function of S and goes to zero smoothly as $S \rightarrow S_c$. This same stress S_c is necessary to initiate the motion of the dislocation from rest.

It was empirically found that all the simulation results obtained for different η_0 and γ values ($\gamma > 2$) could be superimposed after a renormalization into

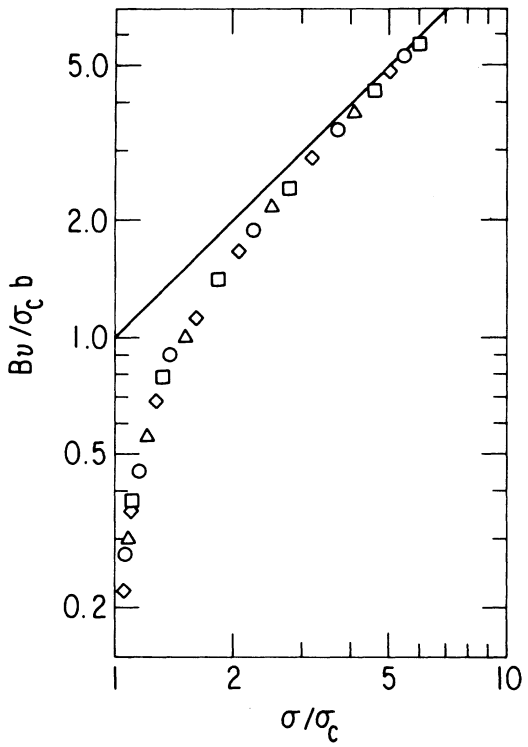

FIG. 5. Dislocation velocity (in units of $\sigma_c b/B$) as a function of the applied stress (in units of σ_c). The solid line gives the viscous drag component. ◇: $\eta_0 = 0.5$, $\gamma = 2$; 0: $\eta_0 = 0.5$, $\gamma = 3$; □: $\eta_0 = 0.5$, $\gamma = 5$; and Δ: $\eta_0 = 2.5$, $\gamma = 3$.

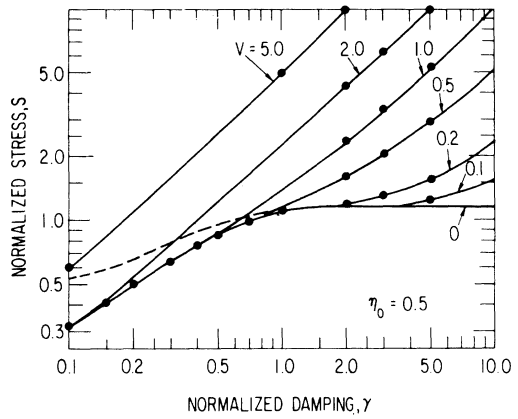

FIG. 6. Constant dislocation velocity curves for obstacles with the interaction profile of Fig. 2(c) and $\eta_0 = 0.5$.

$\gamma V/S_c$ as a function of S/S_c, as shown in Fig. 5. This suggests that for $\gamma > 2$, $V(S)$ has the simple form

$$\frac{\gamma V}{S_c} = f\left(\frac{S}{S_c}\right) , \tag{14}$$

or, in terms of physical units

$$\frac{Bv}{b\sigma_c} = f\left(\frac{\sigma}{\sigma_c}\right) . \tag{15}$$

The computer simulation results for obstacles with the smooth interaction profile of Fig. 2(c) and $\eta_0 = 0.5$ are summarized in Fig. 6. The solid lines give the stress (normalized units) necessary to *maintain* a dislocation in motion at the specified normalized velocity V. The dashed curve is the previously found[8] critical stress S_c necessary to *initiate* the motion from rest, starting in a quasistraight position. The underdamped regime ($\gamma < 1$) is clearly characterized by a static frictional stress larger than the lowest possible dynamic frictional stress.

V. DISCUSSION

A. Critical velocity for $\gamma << 1$

The present calculations and computer simulations show that for $\gamma << 1$, a dislocation can only move at a normalized velocity larger than a critical value $V_L \approx 1$. The origin of this critical velocity can be better understood by analyzing the kinetics of flow for the simplest case of pointlike obstacles, which in our units requires $\eta_0 = 0$.[8] Consider first a plane devoid of obstacles, on which a dislocation parallel to the ξ axis glides in the $+\eta$ direction at the drag-limited velocity V under an applied stress $S = \gamma V$. Assume now that at time $\theta = 0$ this dislocation reaches an impenetrable point barrier located at

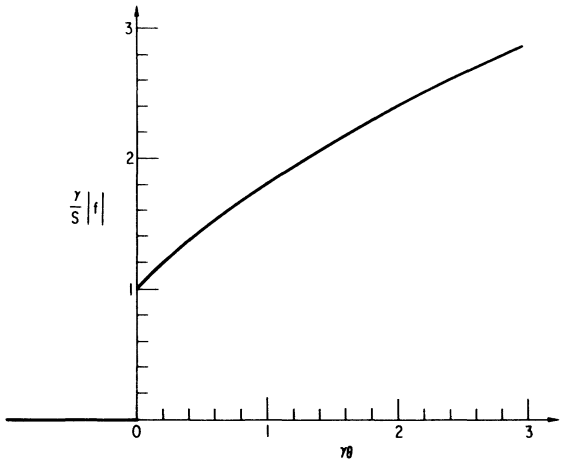

FIG. 7. Time dependence of the force exerted on an impenetrable barrier by a dislocation. A stress S is applied. Prior to the collision the dislocation was moving at the drag-limited velocity, S/γ.

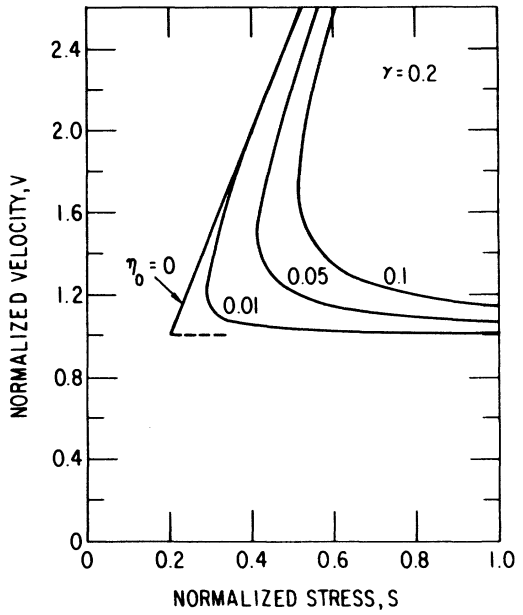

FIG. 8. Velocity-stress dependence (normalized units) for a dislocation interacting with point obstacles and obstacles having the square interaction profile of Fig. 2(a).

$\xi = \eta = 0$. The force $f(\theta)$ that the dislocation exerts on the barrier for $\theta > 0$ has been calculated in the Appendix and is shown in Fig. 7. This curve shows that if the barrier were, instead, a point obstacle of strength unity, one of two distinct situations would result, depending on the value of V.

(a) If $V \geq 1$ the collision has zero duration. The dislocation overcomes the obstacle (of strength unity) on impact and continues its motion unperturbed, as if the point obstacle had not been there. Certainly this is also true when the glide plane contains not one, but a random distribution of point obstacles. Therefore, the flow stress for a dislocation in motion at a velocity $V \geq 1$ through a random array of pointlike obstacles is purely viscous, and $S = \gamma V$ (see Fig. 8). We further note that this result is valid whenever $V > 1$, irrespective of the numerical value of γ.

(b) If $V < 1$ the dislocation cannot surmount the first-point obstacle on impact. The results of the calculation in the Appendix show that this isolated obstacle will be overcome at a later time, as soon as the force on the obstacle exceeds unity. Since the collision time is now finite, a perturbation will be generated on the dislocation, which will tend to retard its motion (see Fig. 1). If the glide plane contains a random obstacle distribution, the situation is further complicated by the fact that the collisions may not be independent. However, since energy is being spent to generate these perturbations, the flow stress for an average velocity $V < 1$ is necessarily larger than the viscous component γV, as shown in Fig. 8.

In conclusion, for $V > 1$ and under a prescribed applied stress, a dislocation moves through a field of point obstacles at the drag-limited velocity S/γ. The stress necessary to start the motion from rest is S_c, which for $\gamma \ll 1$ depends on the statistics of the obstacle distribution (different for a square obstacle array than for a random one, for example) but not on γ.[8] The applied stress at which the motion stops is $S_L = \gamma$ (in physical units, $\sigma_L = B v_s f_0 / b$), which is independent of the obstacle statistics. As previously noted,[8] "dislocation inertial effects"[12,13] appear for $\gamma < 1$ because in this case, S_L becomes smaller than S_c. The present simple description of inertial effects in the presence of point obstacles differs from that proposed in previous theories,[12,13] and yields exact results.

Nothing has been said here about the initiation of the motion, from the instant the dislocation is released from rest by the critical applied stress S_c until it reaches the average velocity $V(S_c)$, close to the drag-limited velocity S_c/γ. Indenbom and Estrin[14] have addressed this problem using a model in which the dislocation, initially at rest against a row of equidistant point obstacles, is released *simultaneously* from all obstacles. Their results, expressed in the present units, show that for $S \approx 1$ and $\gamma \ll 1$ the dislocation reaches a velocity equal to unity (necessary for surmounting obstacles on impact) after traveling a distance much smaller than the average separation between the obstacles. Our computer simulations (see also Ref. 8) show, however, that for a random two-dimensional distribution of obstacles on the glide plane the motion is initiated by the breakway from *one* obstacle and follows by the lateral unzipping of the dislocation from the others along its length. For $\gamma \ll 1$ the forward acceleration at the unzipping front increases continuously and the dislo-

cation is thus able to reach the high velocities necessary to overcome new obstacles on impact. A detailed discussion of this mechanism is forthcoming.[15] The threshold average velocity derived in Ref. 14 also depends on the obstacle separation (owing to the particular initial conditions chosen) and does not correspond to the presently calculated V_L.

The point-obstacle limit ($\eta_0 = 0$) is approached only in the case of extremely dilute alloys.[16] For all other alloys, $\eta_0 > 0$ and the point-obstacle approximation is no longer valid. When $\eta_0 > 0$, the collisions always have a finite duration and the flow stress is necessarily larger than γV. Figure 8 shows $S(V)$ evaluated from Eq. (10) for obstacles having the square interaction-force profile of Fig. 2(a), with increasing η_0 values and $\gamma = 0.2$. The lowest possible dislocation velocity $V_L(\eta_0, \gamma)$ is of order unity. Using the definitions of Sec. II, this means physical velocities $v > v_s f_0$. For an fcc substitutional alloy, where f_0 is typically 0.02, $v > \frac{1}{50} v_s$.

B. Traveling perturbations

Each extended obstacle overcome by the dislocation generates on it two traveling disturbances (Fig. 1). Their amplitude is attenuated as $\exp(-\gamma\xi)$, where ξ is the distance traveled by the perturbations. Their energy is therefore largely dissipated over distances of order $1/\gamma$. Since in our normalized units these disturbances propagate along the dislocation at speed unity while the dislocation glides forward at average speed V, the traveling disturbances can only reach and possibly influence the overcoming of obstacles located along two bands of width $2\eta_0$ forming an angle V with the ξ axis in the direction of forward motion. The average separation between obstacles along these bands is $1/(2\eta_0)$. Therefore, whenever

$$\gamma >> 2\eta_0 \ , \tag{16}$$

the collisions should behave largely as independent. When the above condition is not obeyed, and as a result of all previous collisions, the dislocation velocity as it approaches an obstacle is $V + V_1(\theta)$, where V_1 is a random function of time with an average value of zero. Equation (16) is certainly not fulfilled for the results shown in Fig. 3, obtained with $\eta_0 = 0.5$ and $\gamma = 0.1$. However, the calculations assuming independent collision events (Sec. III A) and the results from the dynamic computer simulation (Sec. III B) coincide not only for V approaching the viscous drag limit, but for all velocities above V_L. This indicates that whenever the S and γ values are such that the result is a continuous dislocation motion everywhere, the presence of traveling perturbations on the dislocation has, on the average, no apparent effect on the collisions and hence on the flow stress.

C. Temperature dependence of $V(S)$

Temperature can affect the dislocation motion mainly in two ways[17]: (a) by an increase in the viscous forces, as a result of the increase in the phonon density, and (b) by the generation of random traveling waves on the dislocation line, via stress fluctuations associated with the lattice thermal fluctuations. The above calculations and simulations have given the velocity-stress dependence in the presence of viscous forces but in the absence of thermal fluctuations. The only way the effect of thermal fluctuations can be rigorously treated is to include them in the computer simulations.[15] In what follows, we discuss, in general terms, the effect that thermal fluctuations can have on the present $V(S)$ dependence.

For $\gamma << 1$ the computer simulations of random arrays of obstacles show that the dislocation travels at high average velocities ($V > 1$), overcoming each obstacle without regard for the positions of the adjacent ones. Furthermore, as discussed in Sec. V B, the traveling perturbations generated by previous collisions seem to have no effect on future collisions. Since the traveling perturbations introduced by temperature-related stress fluctuations are similar in nature to those generated by the superposition of previous dislocation-obstacle collisions, it becomes apparent that for $\gamma << 1$, and for all values of V, only the first effect, the direct $\gamma[B(T)]$ dependence, should have an effect on $V(S)$. The results of Sec. IV A should therefore remain unchanged for finite temperatures.

For $\gamma \gtrsim 2$ (overdamped dislocations) and $V > S_c/\gamma$ [or, in physical units, $v > \sigma_c(T=0)b/B$], the simulations show that the motion is also continuous; the dislocation travels at high velocities ($V \gtrsim 1$), overcoming each obstacle on impact, in complete analogy to the motion for $\gamma << 1$. Therefore, as in the case $\gamma << 1$, thermal fluctuations should again have no influence on the flow stress.

For $\gamma \gtrsim 2$ and $V < S_c/\gamma$ the effect of temperature is more complicated. Thermal fluctuations allow dislocation motion under an applied stress $S < S_c(T=0)$. Here the motion is jerky, and sections of the dislocation spend a time fraction t_w (physical units) waiting for thermally-activated release from strong configurations of obstacles and a time fraction t_r in motion between these configurations. The average velocity (in physical units) is

$$\frac{1}{v} = \frac{t_w}{d} + \frac{t_r}{d} = \frac{1}{v_w} + \frac{1}{v_r} \ , \tag{17}$$

where d is the average separation between the obstacle configurations at which the dislocation stops. The present calculations give v_r for the case $t_w << t_r$ and, as discussed above, temperature should only affect v_r

through $B(T)$. Previous computer simulations[18] and theories[19] have addressed the calculation of v_w for the case $t_w >> t_r$. No consistent treatment, including the appropriate statistics, has been given for the transition regime. However, Eq. (17) and the above discussion indicate that for $v < \sigma_c(T=0)b/B$, v should tend asymptotically to v_w while for $v > \sigma_c(T=0)b/B$, v should tend asymptotically to the presently calculated v_r.

Ney, Labusch, and Haasen[20] have extended the previous calculations of v_w by Haasen *et al.*[19] to higher velocities by adding to the flow stress calculated in the absence of viscous forces [Eq. (25) in Ref. 19] a frictional stress Bv/b. We note that in the limit of high velocities [$v >> b\sigma_c(T=0)/B$], the resultant flow stress does not tend asymptotically to the value Bv/b, as discussed above.

D. Comparison with experiments

The most direct comparison between the present calculations and experiments is provided by direct dislocation-velocity measurements obtained with stress pulses and the double-etch technique.

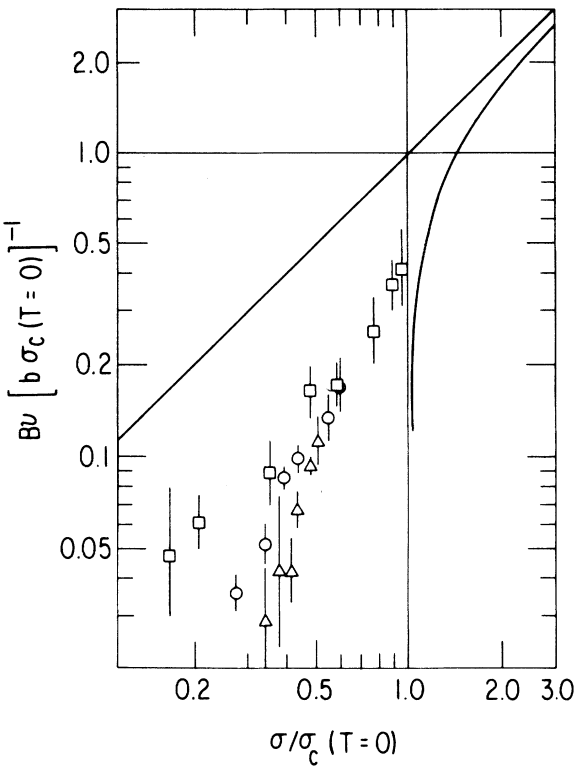

FIG. 9. Dislocation velocities observed in *Cu*-Al alloy crystals by Ney and co-workers (Ref. 20), normalized according to Eq. (15). Solute content (at.%): □, 0.24; ○, 0.75; and Δ, 1.29. The solid diagonal line corresponds to pure viscous drag and the solid curve is the present result in the absence of thermal activation (see Fig. 5).

a. $\gamma << 1$. No direct $v(\sigma)$ measurements appear to have been made in alloys for $T \lesssim 50$ K, where γ may be less than 1 and where the present calculations indicate that dislocations can only move at velocities *higher* than a critical velocity of order $f_0 v_s$. Indirect measurement[21] in Cu - 10.5 at.% Al alloys at 4.2 K give $v \approx 2 \times 10^4$ cm s^{-1} ($\approx \frac{1}{10} v_s$).

b. $\gamma \gtrsim 2$. The only systematic dislocation-velocity measurements in fcc alloys at high temperatures in the velocity regime of present interest are those of Ney, Labusch, and Haasen[20] in dilute Cu-Al alloys at 300 K. In order to normalize their data according to Eq. (15), we need $\sigma_c(T=0)$. Careful measurements of the critical resolved shear stress (CRSS) at 4.2 K are available,[22] although they may not be a good measure of $\sigma_c(T=0)$ if, as we expect,[23] inertial effects are present in dilute fcc alloys at low temperatures.[24] If the measurements for different solute concentrations[20] are normalized using the CRSS[22] at 4.2 K, and $B = 3 \times 10^{-5}$ N s m^{-2} (derived from these same measurements[20]), the resultant data (shown in Fig. 9) seem to asymptotically converge, at high velocities, toward the present result for overdamped dislocations ($\gamma > 2$) in the absence of thermal fluctuatons. This is in agreement with our previous discussion (Sec. V C.)

E. Other friction mechanisms

In the present work we have calculated the dynamic friction arising from the excitation of perturbations on the dislocation as it crosses over fixed obstacles. Other possible dissipative mechanisms are discussed next and compared in importance with the one treated here.

(i) Several authors[1,25–27] have considered the excitation of the quasilocalized vibrational modes of the solute atoms. Numerical estimates[27] indicate, however, that the maximum energy loss per impurity atom is of order 10^{-3} eV and hence two orders of magnitude smaller than the energy (physical units) $\Delta W = \sigma b l_s^2 = 4S\mu b^3 f_0/\eta_0 \approx 0.4$ eV transferred per collision event to the dislocation line. Hence, this resonance should contribute very little to the flow stress. For this numerical estimate of ΔW, we used $S = 0.5$ (contribution of the extrinsic losses to the flow stress of an overdamped dislocation for $V = 1$; see Fig. 5), $\mu b^3 = 5$ eV, $f_0 = 0.02$, and $\eta_0 = 0.5$.

(ii) In extended dislocations there exists the possibility of exciting localized vibrations between the partials. For a dislocation moving at a velocity $v = f_0 v_s \approx \frac{1}{50} v_s$, the collision of each partial with a fixed solute has an approximate duration of $y_0(f_0 v_0)^{-1} \approx 100 b/v_s \approx 10^{-11}$ s. Since the eigenfrequencies of the partials are of order 10^{-10} s,[28] and thus much lower than the Debye frequency, the impulse forces

developed between the solute atoms and the moving dislocation should be able to excite the resonances between the partials more effectively than those of the solute atoms. However, the fact that "inertial effects" are clearly observed in many dilute alloys[23] is indicative of the lack of large extrinsic losses. Thus, this mechanism is also expected to contribute very little to the flow stress.

(iii) Several authors have calculated the dynamic frictional stress in the presence of radiation losses caused by the discreteness of the lattice through which the dislocation moves. Both continuum models (with the addition of phenomenological Peierls potentials) and discrete lattice techniques have been used.

Al'shitz *et al.*[29] found, in agreement with an earlier calculation of Hart,[30] that at high velocities the flow stress in the presence of a Peierls potential decreases as v^{-2}. In the limit of low-viscous forces, the dynamic Peierls stress and the present results show some interesting similarities. For example, the lowering of the average velocity under a decreasing applied stress is possible only down to a critical velocity, at which point the motion stops abruptly. In fcc alloys, with very low Peierls barriers, this dynamic frictional stress should be negligible compared to that due to the solutes, discussed in the present paper. For bcc alloys, both effects should be considered.

Celli and co-workers[31] used discrete lattice techniques to calculate the radiation losses caused by the rearrangement of the atoms in the core of a moving screw dislocation. The applied stress necessary to maintain the motion at a prescribed velocity was found to be highly dependent (varying by more than three orders of magnitude) on the shape of the interatomic forces assumed in the calculations. In view of the uncertainties about these forces, no order-of-magnitude estimate of this frictional force in real crystals can be made.

ACKNOWLEDGMENTS

This work was supported by the U.S. DOE. The author is grateful to W. E. Nixon and J. W. Mitchell for providing their unpublished data for the CRSS stress of Cu-Al alloys at 4.2 K. He also acknowledges useful discussions with U. F. Kocks, R. Labusch, H. Mecking, R. O. Scattergood, and A.P.L. Turner.

APPENDIX

We consider a straight dislocation parallel to the ξ direction, moving in the $+\eta$ direction at the drag-limited velocity V under the applied stress $S=\gamma V$. At time $\theta=0$ the dislocation reaches an impenetrable point barrier located at $\xi=\eta=0$. We calculate the force $f(\theta)$ exerted by the dislocation on this barrier.

The dislocation response to a point force is given by the Green's function for the attenuated string [Eq. (12)]. The dislocation response to the interaction force, when superimposed onto the motion prior to the collision, gives

$$\eta(\xi=0,\theta)=\frac{S}{\gamma}\theta+\int_0^{\theta} f(\theta')e^{-\gamma(\theta-\theta')} \times I_0(\gamma(\theta-\theta'))\,d\theta' \quad . \tag{A1}$$

Since the barrier has zero compliance, $\eta(\xi=0, \theta>0)=0$. Imposing this condition on Eq. (A1), we obtain for $f(\theta)$ a Volterra integral equation of the first kind,

$$-\frac{S}{\gamma}\theta=\int_0^{\theta} f(\theta')e^{-\gamma(\theta-\theta')} \times I_0(\gamma(\theta-\theta'))\,d\theta' \quad . \tag{A2}$$

By taking the Laplace transform ($\theta\rightarrow\mu$) and rearranging terms, we obtain

$$\mu F(\mu)+\frac{S}{\gamma}=-\frac{S}{\gamma}\left(\frac{\mu+2\gamma}{\mu}\right)^{1/2}-1 \quad , \tag{A3}$$

where $F(\mu)$ is the Laplace transform of $f(\theta)$. Since $f(\theta=+0)=-S/\gamma$ [this result follows from Eq. (A2)], the inverse transformation gives

$$\frac{df}{d\theta}=-Se^{-\gamma\theta}[I_0(\gamma\theta)+I_1(\gamma\theta)] \quad . \tag{A4}$$

Finally, an integration from 0 to θ gives

$$f(\theta)=-\frac{S}{\gamma}\left[1+\int_0^{\gamma\theta} e^{-x}[I_0(x)+I_1(x)]\,dx\right] \quad . \tag{A5}$$

The integral in Eq. (A5) was solved numerically, and the result is shown in Fig. 7.

[1]J. Takamura and T. Morimoto, J. Phys. Soc. Jpn. 18, 28 (1963).
[2]A. Aokawa and K. Yazu, J. Phys. Soc. Jpn. 18, 36 (1963).
[3]F.R.N. Nabarro, Z. S. Basinski, and R. Pascual, Scr. Metall. 12, 931 (1978).
[4]Z. S. Basinski, R. A. Foxall, and R. Pascual (unpublished) (see Ref. 3).
[5]H. J. Frost and M. F. Ashby, J. Appl. Phys. 42, 5273 (1971).
[6]U. F. Kocks, A. S. Argon, and M. F. Ashby, in *Progress in Materials Science*, edited by B. Chalmers, J. W. Christian, and T. B. Massalski (Pergamon, New York, 1975), Vol. 19, p. 85.
[7]R. Labusch and R. B. Schwarz, Nucl. Metall. 20, 650

(1976).
[8]R. B. Schwarz and R. Labusch, J. Appl. Phys. 49, 5174 (1978).
[9]P. M. Morse and H. Feshbach, *Methods of Theoretical Physics* (McGraw-Hill, New York, 1953), p. 128.
[10]The extrinsic losses in Eq. (10) can be also derived by computing the kinetic and potential energies of the two traveling waves (see Fig. 1) leaving the collision site.
[11]See Ref. 9, p. 140.
[12]A. V. Granato, Phys. Rev. B 4, 2196 (1971).
[13]M. Suenaga and J. M. Galligan, Scr. Metall. 5, 63 (1971).
[14]V. L. Indenbom and Yu. Z. Estrin, J. Low Temp. Phys. 19, 83 (1975).
[15]R. Labusch and R. B. Schwarz (unpublished).
[16]From Sec. II, $\eta_0 = y_0(l_s\sqrt{f_0})$. Taking $y_0 = 3b$, $l_s = b\sqrt{c}$, and $f_0 = 0.02$ (typical of a substitutional fcc alloy) gives $\eta_0 = 21\sqrt{c}$. Thus, a solute concentration of only 23 ppm already means $\eta_0 = 0.1$.
[17]The temperature dependence of the elastic constants is neglected here. See also Ref. 6, chaps. 4 and 6.
[18]J. W. Morris, Jr., and Dale H. Klahn, J. Appl. Phys. 45, 2027 (1974).
[19]P. Haasen, R. Labusch, G. Grange, and J. Ahearn, in *Rate Processes in Plastic Deformation of Materials*, edited by J. C. M. Li and A. K. Mukherjee (American Society for Metals, Cleveland, 1975), p. 26.
[20]H. Ney, R. Labusch, and P. Haasen, Acta Metall. 25, 1257 (1977).
[21]R. B. Schwarz and J. W. Mitchell, Phys. Rev. B 9, 3292 (1974).
[22]W. E. Nixon and J. W. Mitchell (unpublished data).
[23]R. B. Schwarz, R. V. Isaac, and A. V. Granato, Phys. Rev. Lett. 38, 554 (1977).
[24]In the presence of inertial effects, the macroscopically-measured flow stress of an alloy at a given plastic deformation rate should be some combination of the stress σ_c at which the dislocations start moving, and the stress σ_L at which they stop moving ($\sigma_L < \sigma_c$).
[25]B. Ya. Lyubov and G. M. Chernizer, Sov. Phys. Dokl. 10, 372 (1965).
[26]A. M. Kosevich and V. D. Natsik, Sov. Phys. JETP 24, 810 (1967); Sov. Phys. Solid State 10, 1220 (1968).
[27]M. I. Molotskii, Sov. Phys. Solid State 16, 1637 (1975).
[28]H. Kronmüller, Phys. Status Solidi (b) 52, 23 (1972).
[29]V. I. Al'shitz, V. L. Indenbom, and A. A. Shtol'berg, Sov. Phys. JETP 33, 1240 (1971).
[30]E. W. Hart, Phys. Rev. 98, 1775 (1955).
[31]S. Crowley, N. Flitzanis, and V. Celli, Phys. Chem. Solids 39, 1083 (1978); see also references therein.